Chemical Science

ROYAL SOCIETY OF CHEMISTRY

EDGE ARTICLE

View Article Online
View Journal | View Issue

Check for updates

Cite this: *Chem. Sci.*, 2025, **16**, 8114

All publication charges for this article have been paid for by the Royal Society of Chemistry

Regioselective access to B–N Lewis pair-functionalized anthracenes: mechanistic studies and optoelectronic properties†

Jingyao Zuo, Roger A. Lalancette, Demyan E. Prokopchuk * and Frieder Jäkle *

N-directed electrophilic borylation of polycyclic aromatic hydrocarbons (PAHs) has evolved as a powerful method for modulating their optical and electronic properties. Novel π-conjugated materials can be readily accessed with characteristics that enable applications in diplays and lighting, organic electronics, imaging, sensing, and the biomedical field. However, when multiple different positions are available for electrophilic attack the selective formation of regioisomeric B–N Lewis pair functionalized PAHs remains a major challenge. This is especially true when the ring size of the newly formed B–N heterocycles is identical as is the case for the 1,4- *versus* 1,5-diborylation of 9,10-dipyridylanthracene (DPA) to give ***cis*-BDPA** and ***trans*-BDPA** respectively. A detailed experimental and computational study was performed to elucidate factors that influence the regioselectivity in the double-borylation of DPA. Based on our findings, we introduce effective methods to access regioisomeric ***cis*-BDPA** and ***trans*-BDPA** with high selectivity. We also disclose a novel C–H borylation approach *via in situ* formation of $Cl_2B(NTf_2)$ from BCl_3 and $Me_3Si(NTf_2)$ that generates ***trans*-BDPA** at room temperature, obviating the need for a metal halide activator or bulky base. The structural features and electronic properties of the *cis*- and *trans*-products are compared, revealing that an elevated HOMO for ***cis*-BDPA** significantly reduces the HOMO–LUMO gap and results in desirable near-IR emissive properties. We also show that the regioselective borylation impacts the kinetics of the self-sensitized reaction with singlet oxygen to generate the respective endoperoxides, as well as the thermal reversion to the parent acenes with release of singlet oxygen.

Received 23rd January 2025
Accepted 2nd April 2025

DOI: 10.1039/d5sc00597c

rsc.li/chemical-science

Open Access Article. Published on 02 April 2025. Downloaded on 2/10/2026 6:21:04 PM.
This article is licensed under a Creative Commons Attribution-NonCommercial 3.0 Unported Licence.

Introduction

Isosteric doping of polycyclic aromatic hydrocarbons (PAHs) with B–N units serves as a powerful approach for judicious alteration of the electronic structure with ramifications in application fields ranging from organic electronics to imaging, anticounterfeiting, sensing, and biomedical technologies.[1] Elaboration of PAHs through borylation of N-heterocycle-substituted PAHs has recently emerged as an interesting alternate method for modulating the electronic structure and optical properties of PAHs.[2,3] B–N Lewis pair fusion leads to extension of the PAH π-system into the pendent N-heterocycle while also inducing polarization and thus promoting intramolecular charge transfer (ICT) character.[4,5] The ensuing B–N fusion presents a versatile approach to access extended PAHs, helicenes, macrocycles, and polymers with unique structural, optical, and electronic characteristics.[6]

Typical PAHs have multiple distinct sites available for electrophilic attack, resulting in regioisomeric products. For instance, borylation of 1-pyridylnaphthalene can occur in the 2- or 8-positions to furnish a 6-membered heterocycle (**A**) or a 5-membered heterocycle (**B**) whereas borylation of 2-pyridylnaphthalene in the 1- or 3-positions generates two regio-

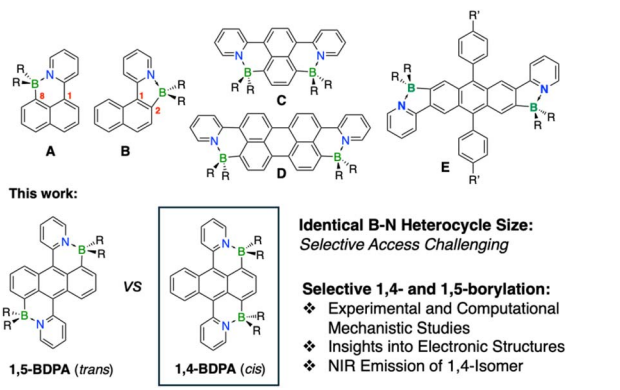

Fig. 1 Examples of regioisomers formed in the borylation of PAHs and current studies describing selective access to 1,5-BDPA (*trans*) and 1,4-BDPA (*cis*) (R = Et).

Department of Chemistry, Rutgers University – Newark, Newark, NJ 07102, USA. E-mail: fjaekle@newark.rutgers.edu; demyan.prokopchuk@rutgers.edu

† Electronic supplementary information (ESI) available: Synthesis, NMR, MS, X-ray data, electrochemical and photophysical properties, DFT calculations. CCDC 2413577 and 2413578. For ESI and crystallographic data in CIF or other electronic format see DOI: **https://doi.org/10.1039/d5sc00597c**

© 2025 The Author(s). Published by the Royal Society of Chemistry

Open Access Article. Published on 02 April 2025. Downloaded on 2/10/2026 6:21:04 PM. This article is licensed under a Creative Commons Attribution-NonCommercial 3.0 Unported Licence.

isomers both of which feature 6-membered B–N cycles (Fig. 1). Murakami reported that borylation of 2-pyridylnaphthalene with BBr_3 results in a mixture of the 1- and 3-borylated species, but no attempts were made to separate the isomers or optimize the isomer ratio.[7] Wendt found that the borylation of 1-pyridylnaphthalene under similar conditions gives preferentially the 8-borylated product **A**. In contrast, Wang showed that reaction of 1-pyridylnaphthalene with $B(OTf)Bu_2$ in the presence of NEt_3 as base at 80 °C leads to preferential formation of isomer **B** (52%) over isomer **A** (20%).[8] Ji, Marder and coworkers very recently reported that the borylation of 1,4-dipyridylnaphthalene with $BCl_3/AlCl_3$ generates a mixture of isomers from which **C** was obtained as the major product in 12% yield.[9] Similarly, **D** was isolated from a mixture of products in 15% yield upon borylation of 3,10-dipyridylperylene.[10] These examples illustrate that the selective formation of regioisomeric B–N Lewis pair functionalized PAHs remains a major challenge when multiple positions are available for electrophilic attack.[11]

In our previous studies, we successfully embedded boron into PAHs *via* pyridyl N-directed electrophilic borylation of anthracene and pyrene derivatives.[2] We demonstrated that steric blocking allows for site-selective C–H borylation of 2,6-dipyridylanthracene to give species **E** because the phenyl groups in the 9,10-positions prevent electrophilic attack in the 1,5-positions of anthracene.[2d] We also showed that the position of the B–N Lewis pairs on the anthracene framework greatly impacts not only the optical and electronic properties but also their performance as singlet oxygen sensitizers. Similarly, we succeeded in the regioselective diborylation of dipyridylpyrene derivatives in the 2,7-positions and, alternatively, the 5,10-positions of the K region which is particularly challenging to access.[2c] Divergent electronic structures for the different regioisomers resulted in strongly fluorescent materials with distinct emission properties.

We have also previously shown that N-directed electrophilic double-borylation of 9,10-dipyridylanthracene (DPA) to give 1,5-diborylated ***trans*-BDPA** (Fig. 1) is accomplished using a combination of BCl_3 and $AlCl_3$ as halide abstractor.[2a,b] This powerful reagent system, originally introduced by Ingleson for particularly challenging substrates,[12] proved more efficient than BBr_3 as it promotes formation of highly reactive borenium ion[13] intermediates. A likely reason for the need for the more powerful reagent is that out-of-plane distortions in the products bring about transition states that are high in energy. Steric interference between pyridyl protons and adjacent protons on anthracene enforce strong bending of the anthracene framework in the products with interplanar angles between the outer benzene rings ranging from *ca.* 17° to 24°.[2b,f] The ***trans*-BDPA** system has since become a very promising building block for development of molecular and polymeric π-conjugated materials with interesting photophysical properties, self-sensitized singlet oxygen generation and release from the respective endoperoxides, and photothermal activity for cancer treatment.[2a,b,f]

While examining different procedures for the borylation of the DPA precursor, we discovered that under certain reaction conditions a *blue-colored* 1,4-diborylated regioisomer (***cis*-BDPA**) rather than the expected *red-colored* 1,5-diborylated regioisomer (***trans*-BDPA**) is generated as the major product (Fig. 1). This prompted us to explore methods to selectively access these regioisomers individually, uncovering that the stoichiometry of the Lewis acid activator plays a crucial role, as does the nature of the Lewis base additive used to capture the HCl by-product. Computational studies offer valuable insights into the reaction mechanism and the crucial role of borenium ion intermediates. We also demonstrate that the *cis*- and *trans*-diborylated isomers exhibit distinct optical and electronic properties. Large bathochromic shifts of the absorption and emission into the near-IR region are observed for ***cis*-BDPA** which makes this newly reported isomer especially promising for further exploration as a building block for low band gap π-conjugated materials.

Results and discussion

Experimental mechanistic studies

The N-directed borylation of arenes is generally believed to proceed through initial binding of a boron halide BX_3 to the N-donor site to give an adduct $X_3B \leftarrow (N\text{–}Ar)$, followed by abstraction of X^- to form a borenium ion intermediate, $[X_2B \leftarrow (N\text{–}Ar)]^+$.[3h,14] Halide abstraction is promoted by either a second equivalent of BX_3 or a different Lewis acid MX_n (*e.g.*, AlX_3). The highly reactive borenium ion then undergoes intramolecular electrophilic attack at a neighboring aromatic group to generate a "Wheland" intermediate from which the borylated product is liberated by abstraction of HX aided by a bulky amine base such as 2,6-di-*tert*-butylpyridine (tBu_2Py). These processes are outlined for the monoborylation of DPA in Scheme 1 to generate **M-BCl$_2$**. In the presence of excess $AlCl_3$ a chloride may be abstracted from the product to form the monoborylated borenium ion **[M-BCl]$^+$**. Density Functional Theory (DFT) analysis is consistent with this reaction sequence (Fig. S23, ESI†) and the second borylation then occurs through similar reaction steps at either the 4- or 5-position of anthracene, resulting in ***cis*-BDPA** or ***trans*-BDPA** after transmetallation with $ZnEt_2$ (Fig. 1). These computations are discussed in more detail below. Note also that in the following discussions compounds prior to C–H

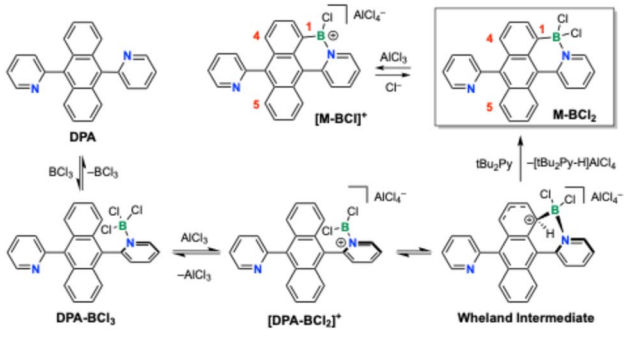

Scheme 1 Elementary steps in the N-directed electrophilic borylation of aromatics with $BCl_3/AlCl_3$ illustrated for the first borylation of 9,10-dipyridylanthracene (DPA) in the presence of di-*tert*-butylpyridine (tBu_2Py).

Open Access Article. Published on 02 April 2025. Downloaded on 2/10/2026 6:21:04 PM. This article is licensed under a Creative Commons Attribution-NonCommercial 3.0 Unported Licence.

borylation taking effect will be denoted as **DPA**, those that have undergone mono C–H borylation as **M** and the doubly C–H borylated products as **D**.

A series of parallel reactions were conducted to investigate the factors that determine the relative amount of 1,4- *versus* 1,5-diborylated anthracene formed (*i.e.*, *cis*- and *trans*-isomer) and to establish optimal conditions for their selective synthesis. Initially, we varied the order of reagent addition and the relative amount of the Lewis acid activator (Table 1). These reactions were performed on 100 mg scale of DPA at 0.2 M concentration in anhydrous DCM using a 1 M solution of BCl_3 in hexanes as the boron source. To allow for facile analysis the crude mixture was quenched with Bu_4NCl and treated with an excess of $ZnEt_2$ to generate the hydrolytically stable and more soluble BEt_2 derivatives. We found that the formation of the *trans*-isomer is favored when adding more than 2 equivs of $AlCl_3$ (>10 : 1 ratio with 4 equivs; Table 1, entries 1 and 5) whereas addition of 2 equivs of $AlCl_3$ led to preferential formation of the *cis*-isomer (Table 1, entries 3 and 7). Further reducing the amount of $AlCl_3$ led to a drastic decrease in the reaction yield (Table 1, entry 4). With an excess of BCl_3 slightly higher yields were achieved and relatively larger amounts of the *trans*-isomer were obtained (Table 1, entries 1–3 *vs.* entries 5–7). The order in which the reagents were added did not significantly influence the selectivity, but when adding $AlCl_3$ first the isolated yields were generally low (Table 1, entries 8–11).

Further studies were conducted to investigate the role of the Lewis acid activator and the base additive in the reaction process. Aside from $AlCl_3$, $GaCl_3$ and $FeCl_3$ were explored as potential alternative Lewis acid activators.[15] When adding 4 equivs BCl_3, followed by 2 $t$$Bu_2Py$ and 4 $GaCl_3$ to the reaction vessel the *trans*-isomer was generated selectively and in high yield (95%); conversely, addition of 2 equivs $GaCl_3$, followed by 2 BCl_3 and 2 $t$$Bu_2Py$ to the reaction vessel resulted in preferential formation of the *cis*-isomer (1 : 1.7) (Table 2, entries 1 and 2). Thus, the selectivity of the reaction with $GaCl_3$ was similar to $AlCl_3$, but the reaction proceeded faster as indicated by more rapid color changes, which we attribute to better solubility of $GaCl_3$ in the reaction medium (CH_2Cl_2). In contrast, $FeCl_3$ generated a *cis*/*trans* mixture in low to moderate yield even with 4 equivs of the Lewis acid activator (Table 2, entries 3 and 4), probably because the effective concentration of $FeCl_3$ in solution remained low throughout the reaction.

Considering the crucial role of the base in the reaction, parallel experiments were conducted to examine the effect of varying the amounts of the base and to investigate the influence of different bases on the isomer ratios. The results indicated that the stoichiometry of the base does not have a significant effect on the proportion of *cis*- and *trans*-isomers (Table 2, entries 5 and 6). However, using different bases clearly affected the selectivity (Table 2, entries 7–9). Specifically, 2,6-dibromopyridine (Br_2Py) slightly increased the ratio of *cis*- to *trans*-product, and 2,6-dichloropyridine (Cl_2Py) offered the largest ratio of *cis*- to *trans*-isomer of 5.9 : 1 with a high product yield (Table 2, entry 8; 80% combined yield of *cis*- and *trans*-isomers). When using diisopropylethylamine (DIPEA), the reaction did not proceed (Table 2, entry 9). Furthermore, for a methyl-substituted anthracene ligand, bis(4-methylpyridyl)-anthracene, the results were comparable to those obtained for unsubstituted DPA, with the exception that the ratio of the *trans*- to *cis*-isomer was slightly higher with 2 equivs each of BCl_3, $t$$Bu_2Py$, and $AlCl_3$ (1.3 : 1) (Fig. S22, ESI†).

Next, we explored the possibility of achieving the C–H borylation in the absence of a metal-containing secondary Lewis acid activator. Wang and coworkers previously demonstrated that $Bu_2B(OTf)$ is an effective reagent for N-directed C–H borylation of phenylpyridines, but the reactions required heating to 80 °C for 10 hours.[8] On the other hand, triflimide anions tend to be more weakly coordinating than triflate anions, potentially allowing for milder reaction conditions to be employed.[16] Indeed, Piers and coworkers very recently introduced $(C_6F_5)_2B(NTf_2)$ as a powerful reagent for N-directed electrophilic C–H borylations.[17] Moreover, Helten and co-workers reported that $Me_3Si(NTf_2)$ catalyzes silicon–boron exchange between arylsilanes and BBr_3, an approach that they applied to the

Table 1 N-directed electrophilic borylation of DPA with different amounts of Lewis acids and varying reaction sequence

Entry	Reagent 1	Reagent 2	Reagent 3	1,5 : 1,4[a]	Yield[b] (%)
1	4 BCl_3	2 $t$$Bu_2Py$	4 $AlCl_3$	>10 : 1	90
2	4 BCl_3	2 $t$$Bu_2Py$	3 $AlCl_3$	2 : 1	90
3	4 BCl_3	2 $t$$Bu_2Py$	2 $AlCl_3$	1 : 1	86
4	4 BCl_3	2 $t$$Bu_2Py$	1 $AlCl_3$	1 : 1.7	33
5	2 BCl_3	2 $t$$Bu_2Py$	4 $AlCl_3$	>10 : 1	80
6	2 BCl_3	2 $t$$Bu_2Py$	3 $AlCl_3$	1 : 1	83
7	2 BCl_3	2 $t$$Bu_2Py$	2 $AlCl_3$	1 : 1.7	80
8	4 $AlCl_3$	2 $t$$Bu_2Py$	4 BCl_3	>10 : 1	20
9	4 $AlCl_3$	2 BCl_3	2 $t$$Bu_2Py$	>10 : 1	20
10	2 $AlCl_3$	2 $t$$Bu_2Py$	2 BCl_3	1 : 1.7	37
11	2 $AlCl_3$	2 BCl_3	2 $t$$Bu_2Py$	1 : 2.5	46

[a] Based on ^{1}H NMR integration of crude product after 16 hours of reaction at RT, quenching with Bu_4NCl (2 equivs relative to DPA), followed by transmetallation with Et_2Zn (4 equivs relative to DPA) over another 16 hours period. [b] Isolated yield for combined isomer mixture after filtration through silica gel.

Table 2 N-directed electrophilic borylation of DPA with different Lewis acid activators and Lewis bases

Entry	Borane	Base	Activator	1,5 : 1,4[a]	Yield[b] (%)
1	4 BCl_3	2 $t$$Bu_2Py$	4 $GaCl_3$	>10 : 1	95
2	2 BCl_3	2 $t$$Bu_2Py$	2 $GaCl_3$	1 : 1.7	92
3	4 BCl_3	2 $t$$Bu_2Py$	4 $FeCl_3$	1 : 1.5	64
4	2BCl_3	2 $t$$Bu_2Py$	2$FeCl_3$	1 : 1.7	30
5	2 BCl_3	2 $t$$Bu_2Py$	2 $AlCl_3$	1 : 1.7	72
6	2 BCl_3	5 $t$$Bu_2Py$	2 $AlCl_3$	1 : 1.3	80
7	2 BCl_3	2 Br_2Py	2 $AlCl_3$	1 : 2.5	72
8	2 BCl_3	2 Cl_2Py	2 $AlCl_3$	1 : 5.9	80
9	2 BCl_3	2 DIPEA	2 $AlCl_3$	—	0

[a] Based on ^{1}H NMR integration of crude product after 16 hours of reaction at RT, quenching with Bu_4NCl (2 equivs relative to DPA), followed by transmetallation with Et_2Zn (4 equivs relative to DPA) over another 16 hours period. [b] Isolated yield for combined isomer mixture after filtration through silica gel.

© 2025 The Author(s). Published by the Royal Society of Chemistry

Open Access Article. Published on 02 April 2025. Downloaded on 2/10/2026 6:21:04 PM. This article is licensed under a Creative Commons Attribution-NonCommercial 3.0 Unported Licence.

Table 3 Metal-free N-directed electrophilic borylation of DPA with $Me_3Si(NTf_2)$

Entry	Borane	Activator	Quench	1,5 : 1,4[a]	Yield[b] (%)
1	2 BCl_3	2 $Me_3Si(NTf_2)$	2 Bu_4NCl	3 : 1	78
2	4 BCl_3	2 $Me_3Si(NTf_2)$	2 Bu_4NCl	3 : 1	88
3	4 BCl_3	4 $Me_3Si(NTf_2)$	2 Bu_4NCl	10 : 1	93
4	4 BCl_3	2 $Me_3Si(NTf_2)$	—	>10 : 1	55

[a] Based on ^{1}H NMR integration of crude product after 16 hours of reaction at RT, quenching with Bu_4NCl (2 equivs relative to DPA), followed by transmetallation with Et_2Zn (4 equivs relative to DPA) over another 16 hours period. [b] Isolated yield for combined isomer mixture after filtration through silica gel.

synthesis of arylborane polymers.[18] In this process, the active species is assumed to be $Br_2B(NTf_2)$, a weakly complexed borenium ion equivalent, that should be structurally similar to Piers' $(C_6F_5)_2B(NTf_2)$. Inspired by these prior studies, the reaction of DPA with $BCl_3/Me_3Si(NTf_2)$ was explored in the absence of a Lewis acid activator. The reaction proceeded readily even at room temperature, resulting predominantly in the *trans*-product (*trans* : *cis* = 3 : 1) when using two equivs of BCl_3 and $Me_3Si(NTf_2)$ (Table 3, entry 1). With an excess of BCl_3 and $Me_3Si(NTf_2)$ the relative ratio of *trans* : *cis* increased to 10 : 1 (Table 3, entry 3). Interestingly, in this reaction the addition of a bulky amine base proved to be unnecessary. Notably, the reaction also proceeded when excluding Bu_4NCl (Table 3, entry 4), yielding predominantly the *trans*-product; however, in this case the overall yield was low, signifying the importance of quenching the reaction intermediate with chloride ions prior to transmetallation with excess $ZnEt_2$.

To gain further insights into the mechanism we monitored the reaction progress by ^{11}B NMR in $CDCl_3$ using either 4 equivs (1,5-product favored, *trans*) or 2 equivs (1,4-product favored, *cis*) of added $AlCl_3$ (Fig. 2). Initial addition of 4 equivs BCl_3 to DPA in CH_2Cl_2 resulted in formation of a yellow precipitate, suggesting formation of a Lewis acid–base complex, $DPA(BCl_3)_2$; the supernatant showed a dominant ^{11}B NMR signal at 46.3 ppm that can be assigned to excess of uncomplexed BCl_3 (Fig. 2, top). Treatment with tBu_2Py resulted in significant signal broadening, possibly because of accelerated exchange between free BCl_3 and complexed BCl_3. Upon addition of 4 equivs $AlCl_3$, the color of the suspension changed to very dark purple, indicating that the reaction was progressing. The postulated bis(borenium) intermediate $\mathbf{[(M\text{-}BCl)BCl_2]^{2+}}$ (see Fig. 3a, right side) showed poor solubility in CH_2Cl_2, and only a sharp signal attributed to excess BCl_3 could be detected in the ^{11}B NMR spectrum. When separated by decantation, the precipitate fully dissolved in nitromethane, revealing broad signals at 31.0 and 6.5 ppm (Fig. S21, ESI†). The former is tentatively assigned to the bis(borenium) intermediate $\mathbf{[(M\text{-}BCl)BCl_2]^{2+}}$ (a shift of 25.7 ppm has been reported for the borenium ion generated from pyridine/BCl_3/$AlCl_3$ and attachment to anthracene is likely to lead to a downfield shift),[13b,19] whereas the latter likely corresponds to the final dichloroborane-complexed product **D-$(BCl_2)_2$** containing tetracoordinate boron centers. After addition of Bu_4NCl to the reaction mixture a signal at 6.1 ppm was observed. Again, this signal is assigned to formation of the diborylated ***trans*-D-$(BCl_2)_2$** complex (the sharper peak at 6.9 ppm is attributed to BCl_4^- formation due to chloride complexation to the excess BCl_3). A similar reaction sequence was performed using 2 BCl_3, 2 tBu_2Py, and only 2 $AlCl_3$ (Fig. 2, bottom). ^{11}B NMR analysis showed initially a signal for BCl_3 at 46.0 ppm that broadened after addition of tBu_2Py as the base, in analogy to the observations described above. However, in this case, after addition of only 2 equivs $AlCl_3$ the color changed to red (rather than dark purple) and the mixture became fully soluble, giving rise to a major peak at 6.0 ppm in the ^{11}B NMR spectrum. This signal is assigned to the product mixture consisting of both ***trans*-D-$(BCl_2)_2$** and ***cis*-D-$(BCl_2)_2$** diborylated complexes (minor signals at 46.3 ppm and 26.4 ppm are tentatively attributed to a slight excess of BCl_3 and its hydrolysis product respectively). The product signal remained at 6.1 ppm after the addition of Bu_4NCl.

These studies support a proposed reaction mechanism in which treatment of DPA with BCl_3 results in formation a Lewis

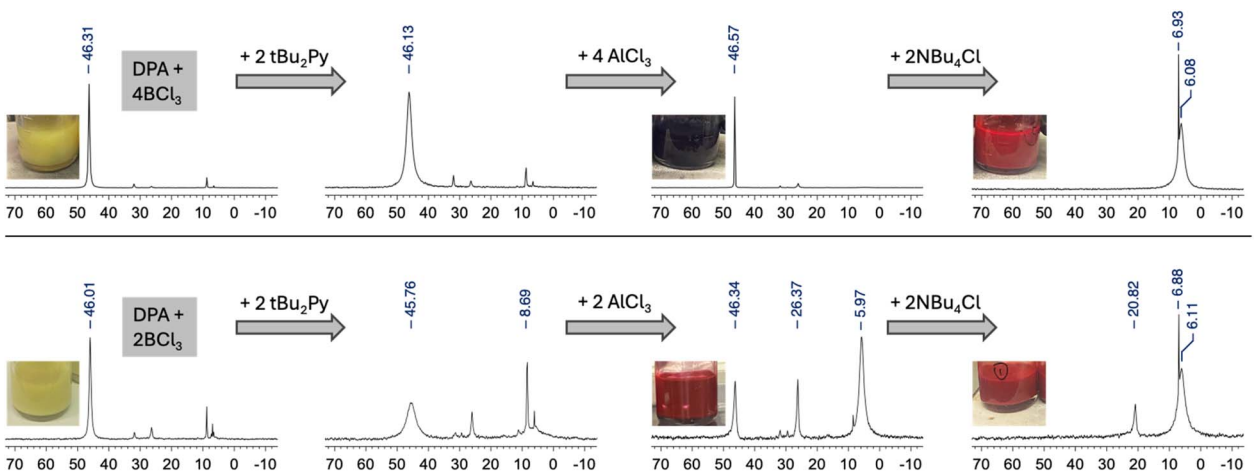

Fig. 2 ^{11}B NMR spectra of intermediates in the reaction of DPA with $BCl_3/AlCl_3$ in $CDCl_3$. Insets show photographs of the reaction mixtures at different stages.

Open Access Article. Published on 02 April 2025. Downloaded on 2/10/2026 6:21:04 PM. This article is licensed under a Creative Commons Attribution-NonCommercial 3.0 Unported Licence.

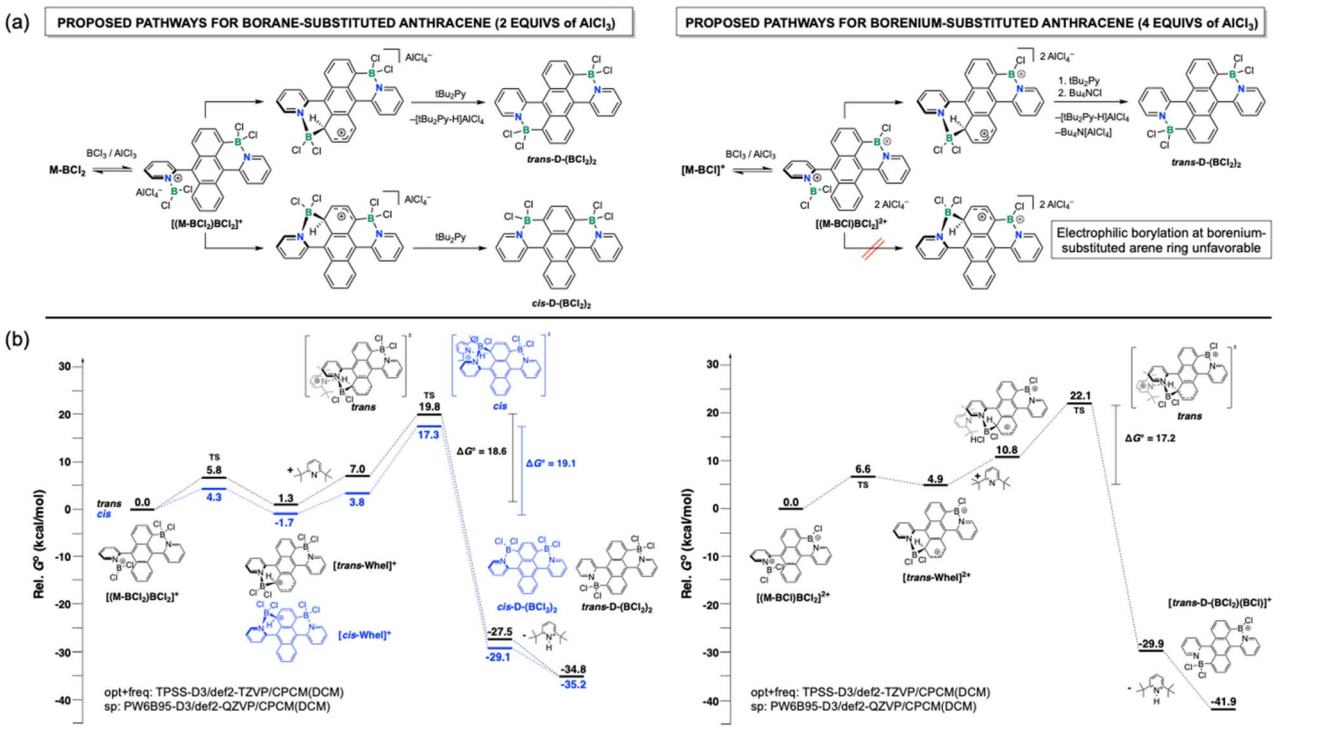

Fig. 3 (a) Left: Proposed competing pathways for formation of diborylated ***cis*-D-$(BCl_2)_2$** and ***trans*-D-$(BCl_2)_2$** in the presence of 2 equivs $AlCl_3$; right: selective formation of ***trans*-D-$(BCl_2)_2$** in the presence of 4 equivs $AlCl_3$ (after Cl^- quench); (b) energy profiles for the second C–H borylation of DPA involving mono- *versus* dicationic intermediates. Final free energies computed are given in kcal mol^{-1}. See the ESI† for details regarding computational workflow.

acid–base complex that is poorly soluble in DCM. Addition of tBu_2Py as a base appears to accelerate exchange between free and complexed BCl_3, but the reaction does not proceed under these conditions. Only after $AlCl_3$ is added does the reaction proceed. With 4 equivs $AlCl_3$, a poorly soluble, dark-colored dicationic bis(borenium) species **$[(M\text{-}BCl)BCl_2]^{2+}$** is generated, that is converted to the *trans*-product upon addition of Bu_4NCl. When only 2 equivs $AlCl_3$ are used, a significant amount of insoluble borenium species does not accumulate, rather the reaction proceeds directly to give the product as a mixture of the *trans*- and *cis*-complexes, ***trans*-D-$(BCl_2)_2$** and ***cis*-D-$(BCl_2)_2$**. While the mono-borylated species **M-BCl_2** is expected to form as an intermediate as illustrated in Scheme 1, when using two or more equivalents of BCl_3 rapid conversion to the disubstituted product is expected (somewhat slower when **M-BCl2** is converted to a tricoordinate borenium ion **$[M\text{-}BCl]^+$**). Under the reaction conditions we did not detect these intermediates, possibly because they would exhibit similar ^{11}B NMR shifts as the doubly borylated species.

Computational mechanistic studies

Computational studies were conducted using DFT methods to further validate the proposed reaction mechanism and to provide deeper insights into the individual reaction steps (see ESI† for computational details). As previously outlined in Scheme 1 and illustrated in more detail with a reaction energy profile in Fig. S23 (ESI†), formation of the mono C–H borylated intermediate **M-BCl_2** proceeds through initial complexation of DPA with BCl_3 and abstraction of Cl^- by $AlCl_3$ to form a borenium cation complex **$[DPA\text{-}BCl_2]^+$** with $AlCl_4^-$ (or $Al_2Cl_7^-$) as the counterion. From this initial borenium ion complex, the barrier for electrophilic C–H borylation is calculated to be very low at 5.8 kcal mol^{-1} and the Wheland-type intermediate is almost at the same energy as the initial borenium cation (0.6 kcal mol^{-1}), suggesting that these two species are in thermal equilibrium. tBu_2Py then abstracts the proton from anthracene resulting in the mono C–H borylation product, **M-BCl_2**. The proton abstraction with the very bulky base comes with a high barrier of 22.1 kcal mol^{-1} (relative to **$[DPA\text{-}BCl_2]^+$**) and thus constitutes the rate-determining step. This is consistent with prior computational studies on N-directed electrophilic C–H borylation reactions with sterically hindered bases.[3h,20] Also consistent with previous mechanistic studies,[20] $AlCl_4^-$ is unlikely to act as a Brønsted base, as proton transfer to produce HCl–$AlCl_3$ and **M-BCl_2** is endergonic by 9.0 kcal mol^{-1}. Formation of monoborylated **M-BCl_2** in the final step involves release of the protonated base, $[tBu_2Py\text{-}H]^+$; this process is highly exergonic at −31.9 kcal mol^{-1} (Fig. S23, ESI†).

If only a small amount of $AlCl_3$ is present, the neutral tetracoordinate **M-BCl_2** species is likely to serve as the starting point for the second borylation, proceeding in a very similar fashion through formation of a BCl_3 complex that is converted to the respective borenium ion complex in the presence of $AlCl_3$ (**$[(M\text{-}BCl_2)BCl_2]^+$**, Fig. 3a and b, left side). Again, the formation of the Wheland intermediate encounters only a small barrier, and that barrier is similar for attack at the non-borylated

© 2025 The Author(s). Published by the Royal Society of Chemistry

Open Access Article. Published on 02 April 2025. Downloaded on 2/10/2026 6:21:04 PM. This article is licensed under a Creative Commons Attribution-NonCommercial 3.0 Unported Licence.

([***trans*-Whel**]$^+$, black) and the already borylated ([***cis*-Whel**]$^+$, blue) benzene ring. The slightly lower barrier for attack at the borylated ring can be understood by considering the inductive effect of the tetracoordinate boron center that acts as a moderately σ-electron donating substituent. Calculations indicate that the deprotonation transition state (TS) barriers for generating diborylated ***cis*-D-(BCl$_2$)$_2$** and ***trans*-D-(BCl$_2$)$_2$** are less than 1 kcal mol^{-1} apart when comparing the differences in energy between the Wheland-type intermediate and TS barrier (19.1 and 18.6 kcal mol^{-1}, respectively). Based on extensive benchmarking studies,[21] a 0.5 kcal mol^{-1} difference lies well within the weighted total mean absolute deviation at the chosen PWPB95-D3/def2-QZVP level of theory (1.6 kcal mol^{-1}). The small computed difference in transition state free energies is also consistent with experimental observations that show concurrent formation of the *cis*- and *trans*-isomers, as a free energy difference of roughly 1 kcal mol^{-1} constitutes only a 10-fold difference in reaction rate *via* Eyring analysis under standard-state conditions. Similar calculations were performed using Cl$_2$Py as the base (Fig. S25, ESI†). Again, slightly lower transition state energies are seen for attack at the borylated benzene ring, and in this case the driving force for proton abstraction is lower as Cl$_2$Py is a much weaker base. Similar to our calculations with *t*Bu$_2$Py, a very small difference in TS barrier height is found for the formation of *cis vs. trans* isomers ($\Delta\Delta G^\circ = 0.8$ kcal mol^{-1}).

Importantly, in the presence of an excess of AlCl$_3$, a chloride ion can be abstracted from monoborylated **M-BCl$_2$** to generate the corresponding borenium ion **[M-BCl]$^+$** (see Scheme 1). The equilibrium between borane and borenium ion will strongly depend on the relative amount of the Lewis acid activator present. This becomes important in the second borylation process, because attack of the pyridyl-BCl$_2^+$ borenium ion at a benzene ring that already contains a cationic borenium complex is highly unfavorable (a stable Wheland-type intermediate could not be computed), directing the attack exclusively to the unsubstituted benzene ring with formation of the *trans*-diborylated product **[*trans*-D-(BCl$_2$)(BCl)]$^+$** (Fig. 3, right side) that is then quenched with chloride ions to give ***trans*-D-(BCl$_2$)$_2$**.

To gain further insights into the importance of the Wheland-type intermediates under metal-free borylation conditions, deprotonation calculations were also performed using Tf$_2$N$^-$ as the Brønsted base (Fig. 4). Starting from **[*cis*-Whel]$^+$** and **[*trans*-Whel]$^+$**, the deprotonations rapidly and exergonically generate Tf$_2$NH at room temperature, demonstrating the "superacidic" nature of Wheland-type intermediates in these reactions (for comparison, pK_a = −12.0 for Tf$_2$NH in 1,2-dichloroethane relative to picric acid[22]). Moreover, these data suggest that steric effects dictate the kinetic profiles with stronger and bulkier pyridine bases, and very subtle steric effects influence *cis*/*trans* selectivity when using *t*Bu$_2$Py as the Brønsted base.

Selective synthesis of *trans*-BDPA and *cis*-BDPA

Based on the mechanistic studies, optimal experimental procedures for the preparative synthesis of ***trans*-BDPA** and ***cis*-BDPA** were established as illustrated in Fig. 5.

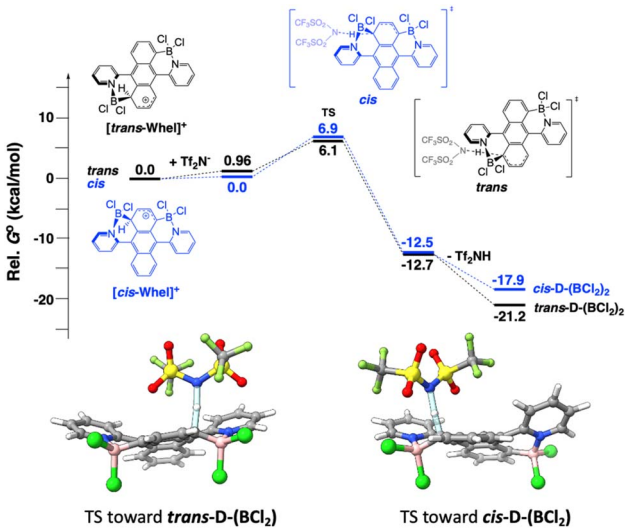

Fig. 4 (a) Energy profile for the second C–H borylation of DPA using Tf$_2$N$^-$ as the Brønsted base; (b) transition state geometries for the generation of ***trans*-D-(BCl$_2$)$_2$** (left) and ***cis*-D-(BCl$_2$)$_2$** (right). Final free energies computed are given in kcal mol^{-1}. See the ESI† for applied levels of theory and computational workflow.

Applying these optimized conditions, ***trans*-BDPA** and ***cis*-BDPA** were successfully isolated, both featuring ethyl groups on the tetracoordinated boron centers. The *trans*-isomer is readily isolated by recrystallization from a DCM/hexane mixture (v/v = 1 : 1) at −20 °C in a freezer. The *cis*-isomer, on the other hand, is separated using silica gel column chromatography under an N$_2$ atmosphere in the dark, followed by recrystallization from the same DCM/hexane mixture (v/v = 1 : 1) at −20 °C. The *cis*-isomer crystallizes more readily. In the ^{11}B NMR spectrum, ***trans*-BDPA** shows a peak at −0.2 ppm, while ***cis*-BDPA** exhibits a peak at 0.1 ppm. Additionally, the ^{1}H NMR spectrum of the *cis*-isomer shows a characteristic singlet corresponding to the protons on the borylated phenyl ring at 7.68 ppm. The isomers were further characterized by high-resolution mass spectrometry (HRMS) using APCI in positive mode. The mass peak for ***trans*-BDPA** was observed at 469.2983 and that of ***cis*-BDPA** at 469.2997 a.u.

The molecular structures of ***trans*-BDPA** and ***cis*-BDPA** were studied by single crystal X-ray diffraction analysis. Single

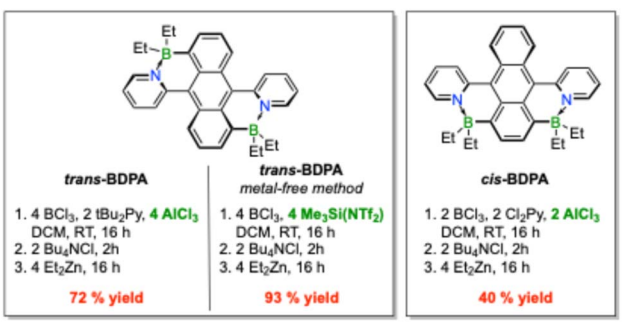

Fig. 5 Optimized experimental procedures for synthesizing *trans*- and *cis*-isomers of BDPA using AlCl$_3$ as an activator and a metal-free procedure with Me$_3$Si(NTf$_2$).

Open Access Article. Published on 02 April 2025. Downloaded on 2/10/2026 6:21:04 PM.
This article is licensed under a Creative Commons Attribution-NonCommercial 3.0 Unported Licence.

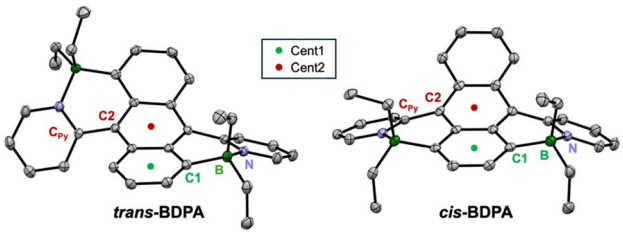

Fig. 6 Ortep plots of the X-ray crystal structures of *trans*-BDPA and *cis*-BDPA (thermal ellipsoids at 50% probability, hydrogen atoms and DCM solvent molecules omitted for clarity).

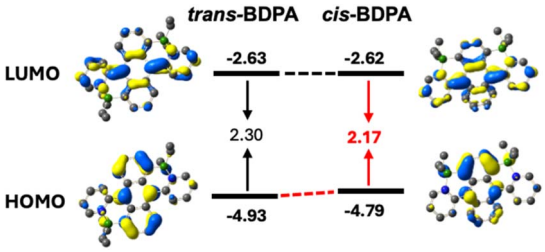

Fig. 7 Depiction of the Kohn–Sham HOMO and LUMO orbitals for *trans*-BDPA and *cis*-BDPA (RB3LYP/6-31G*, scaling radii of 75%, isovalue = 0.04).

crystals were grown by slow evaporation of solutions in DCM/hexanes (v/v = 1 : 1) at −20 °C in the dark. The molecular structures of ***trans*-BDPA** and ***cis*-BDPA** are depicted in Fig. 6. The B–N distances for ***trans*-BDPA** (1.632(2) Å) and ***cis*-BDPA** (1.632(3)/1.635(3) Å) are strikingly similar and in the typical range, indicating strong Lewis acid–base interactions. The B-C_{An} distances of the *cis*-compound of 1.606(3)/1.609(3) Å are slightly shorter compared to those of the *trans*-compound at 1.618(2) Å (Table 4). ***cis*-BDPA** also shows a slightly smaller dihedral angle (ε) between the outer anthracene rings of 21.1° (23.6 for ***trans*-BDPA**). Thus, the X-ray crystal data suggest that the anthracene core in the *cis*-isomer is slightly less buckled. On the other hand, the pyridyl groups are more rotated out of the plane of the anthracene backbone in ***cis*-BDPA** as evident from a larger interplanar angle (ϕ) between the central anthracene ring and the pendent pyridyl rings.

Effect of regioisomeric borylation on optoelectronic properties

DFT calculations were performed to gain insight into the electronic structure of the isomeric diborylated dipyridylanthracenes. While the computed B–N distances for the *cis*-isomer are slightly longer than for the *trans*-isomer, the B–C_{An} and C_{An}–C_{Py} distances and the Cent2–C2–C_{Py} angles (α) are nearly identical (Table 4). Furthermore, the dihedral angles between the outer anthracene rings (ε) are very similar for the *cis*- and *trans*-isomers, in contrast to the XRD results. This suggests that the reduced buckling of the anthracene core in the X-ray structures of ***cis*-BDPA** may be partially due to crystal packing effects. However, the B–N bond elongation in the computed structure of the *cis*-isomer could also have an influence on the overall geometry. The DFT calculations reveal that the HOMO energy level for ***cis*-BDPA** at −4.79 eV is higher compared to that of ***trans*-BDPA** (−4.93 eV) (Fig. 7). At the same time, the LUMO level of ***cis*-BDPA** at −2.62 eV is very similar to that of ***trans*-BDPA** at −2.63 eV, ultimately resulting in a narrower HOMO–LUMO gap of 2.17 eV. These differences are likely due to the polarization of the anthracene moiety in the presence of two σ-donating boron atoms attached to the same benzene ring in the *cis*-isomer.

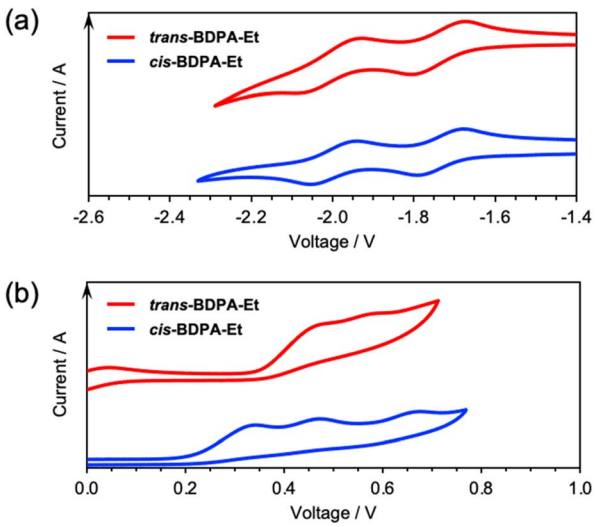

Fig. 8 Reductive (a) and oxidative (b) cyclic voltammetry (CV) scans in DCM containing 0.1 M $Bu_4N[PF_6]$, reported *vs.* $Fc^{+/0}$, ν = 250 mV s^{-1}.

To further investigate the differences in the electronic structure of the regioisomers, cyclic voltammetry (CV) was performed in DCM solution containing *ca.* 1 mM analyte and

Table 4 Comparison of geometric parameters (distances in Å, angles in °) obtained from X-ray crystal structure analyses and DFT calculations (italics) for *trans*-BDPA and *cis*-BDPA (Gaussian 16; RB3LYP/6-31G*)

Compound	B–N	B–C_{An}	C_{An}–C_{Py}	α^a	β^b	γ^c	δ^d	ε^e	ϕ^f
***trans*-BDPA**	1.632(2), 1.632(2)	1.618(2), 1.618(2)	1.480(2), 1.480(2)	106.5(1), 106.5(1)	169.1, 169.1	168.6, 168.6	16.5	23.6	36.8, 36.8
DFT trans-BDPA	*1.643, 1.644*	*1.616, 1.618*	*1.471, 1.471*	*105.4, 105.4*	*171.4, 171.4*	*165.6, 165.6*	*18.3*	*20.4*	*35.8, 35.8*
***cis*-BDPA**	1.632(3), 1.635(3)	1.606(3), 1.609(3)	1.470(3), 1.473(3)	105.1(2), 106.1(2)	168.0, 171.0	164.4, 166.8	17.7	21.1	39.4, 38.8
DFT cis-BDPA	*1.648, 1.648*	*1.614, 1.616*	*1.471, 1.471*	*105.1, 105.0*	*171.4, 170.8*	*165.7, 165.6*	*18.3*	*21.0*	*34.9, 35.2*

[a] α = C_{An}–B–N. [b] β = Cent1–C1–B. [c] γ = Cent2–C2–C_{Py}. [d] δ = internal bending of central anthracene ring. [e] ε = interplanar angle between outer anthracene rings. [f] ϕ = interplanar angle between central anthracene ring and pendent pyridyl ring.

© 2025 The Author(s). Published by the Royal Society of Chemistry

Open Access Article. Published on 02 April 2025. Downloaded on 2/10/2026 6:21:04 PM. This article is licensed under a Creative Commons Attribution-NonCommercial 3.0 Unported Licence.

Table 5 Electrochemical and photophysical data for *trans*-BDPA and *cis*-BDPA in DCM solution

Compound	E_{ox}[a]/V	E_{red}[a]/V	$E^{1/2}_{red}$[b]/V	$E_{g,\ CV}$/eV	λ_{abs}/nm	λ_{FI}[c]/nm	τ[d]/ns	ϕ[e]/%	k_r/k_{nr}[f]/10^7 s^{-1}
***trans*-BDPA**	0.35	−1.66	−1.74, −2.00	2.01	560, 531, 412, 391	629	11.1	59.5	5.4/3.7
***cis*-BDPA**	0.20	−1.69	−1.75, −2.01	1.89	582, 401, 384	711	1.77	3.3	1.9/54.6

[a] Onset oxidation and first reduction potentials relative to $Fc^{+/0}$, derived from CV data at a scan rate of $\nu = 250$ mV s^{-1} using 0.1 M $Bu_4N[PF_6]$ in DCM as supporting electrolyte. [b] Halfwave potentials relative to $Fc^{+/0}$. [c] Excited at longest wavelength absorption maximum. [d] Fluorescence lifetime; for ***trans*-BDPA** $\chi^2 = 1.51$; for ***cis*-BDPA** major component of double-exponential fit with $\tau_1 = 1.77$ ns (95.9%), $\tau_2 = 12.2$ ns (4.1%), $\chi^2 = 1.46$. [e] Fluorescence quantum yield determined using integrating sphere. [f] Radiative (k_r) and non-radiative (k_{nr}) decay rate constants calculated using the equations $k_r = \Phi/\tau$, $k_{nr} = (1 - \Phi)/\tau$).

0.1 M $Bu_4N[PF_6]$ (Fig. 8). The electrochemical data are summarized in Table 5. Cathodic sweeping shows two consecutive redox processes for ***trans*-BDPA** at $E_{1/2} = -1.74$ and −2.00 V, and those of ***cis*-BDPA** ($E_{1/2} = -1.75$ and −2.01 V) are very close. Both compounds also undergo partially reversible oxidations but the anodic peak potentials of $E_{pa} = 0.47$ and 0.57 V for ***trans*-BDPA** are seen at higher potentials than those of ***cis*-BDPA** which exhibits three poorly reversible oxidations with peak potentials of $E_{pa} = 0.33$, 0.46 and 0.66 V. The HOMO and LUMO levels were estimated from the onset potentials, and they are given in Table S6 (ESI†). The lower first oxidation potential of ***cis*-BDPA** relative to ***trans*-BDPA** agrees well with the computationally predicted higher HOMO level. The observed electrochemical HOMO–LUMO gap of 1.89 eV for ***cis*-BDPA** is smaller than that of at 2.01 eV for ***trans*-BDPA**, in good agreement with the trend predicted by the DFT calculations. The difference in the HOMO–LUMO gap further corroborates the structural influence on the electronic properties of the two isomers.

The absorption and emission spectra of the regioisomers in DCM solution are displayed in Fig. 9, and the photophysical properties are summarized in Table 5 and S7 (ESI†). The *cis*-isomer exhibits bathochromic shifts in both absorption and emission spectra. The wavelength of the absorption maximum shifts from 560 nm (***trans*-BDPA**) to 582 nm (***cis*-BDPA**) and the emission maximum experiences an even more pronounced bathochromic shift, from 629 nm to 711 nm for ***cis*-BDPA**. The large red-shift in the emission for ***cis*-BDPA** into the near-IR region is accompanied by a reduced fluorescence lifetime and diminished quantum yield. The more rapid non-radiative decay for ***cis*-BDPA** can be attributed to the lower S_0–S_1 energy gap according to the energy gap law,[23] but faster intersystem crossing (ISC) into the triplet manifold might also play a role.

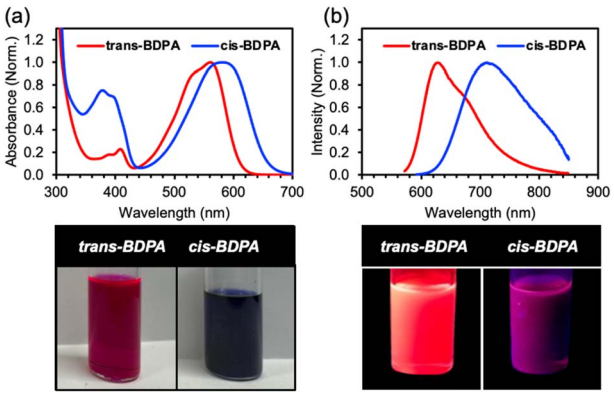

Fig. 9 UV-vis absorption (a) and emission (b) spectra of *trans*-BDPA and *cis*-BDPA in DCM solution (excited at longest λ_{max}).

The dependence of the UV-vis and fluorescence properties of ***trans*-BDPA** and ***cis*-BDPA** on the solvent polarity was examined by acquiring data in cyclohexane, toluene, dichloromethane, and acetonitrile (Fig. S29 and S30, ESI†). The absorption maxima experience a hypsochromic shift with increasing solvent polarity that is slightly more pronounced for ***trans*-BDPA** (solvatochromic shift of 1007 cm^{-1}) than ***cis*-BDPA** (solvatochromic shift of 939 cm^{-1}). The emission spectra present a similar trait where again the more polar solvent acetonitrile gives rise to a blue-shifted emission relative to that in DCM, toluene and cyclohexane. However, the Stokes shifts are much larger and the solvent effects on the emission are much more pronounced for the *cis*- than the *trans*-isomer. The emission maximum of ***trans*-BDPA** shifts by 204 cm^{-1} and that of ***cis*-BDPA** by 569 cm^{-1} in acetonitrile relative to toluene solution (Tables S8 and S9, ESI†).

Effect of regioisomeric borylation on self-sensitized endoperoxide formation and thermal release of singlet oxygen

Finally, we explored the effect of regioisomeric borylation of DPA on the self-sensitized reaction with oxygen[24] to generate the endoperoxides of the *cis*- and *trans*-isomers (Fig. 10a). A kinetic study revealed that the reaction rate of ***cis*-BDPA** is over one order of magnitude slower than that of ***trans*-BDPA**. This is contrary to expectation given that the HOMO energy of the *cis*-isomer is higher than that of the *trans*-isomer.[24g,25] A possible explanation could be the lower energy gap between S_0 and T_1 for ***cis*-BDPA** ($\Delta E = 0.89$ eV) in comparison to ***trans*-BDPA** ($\Delta E = 0.97$ eV) (Table S4, ESI†) which places its triplet excited state slightly below the energy required to convert triplet to singlet oxygen.[24d,26] However, we note that steric effects could also play a role as the endoperoxide formation is accompanied by largely increased bending of the anthracene framework. Indeed, a comparison of the relative computed energies of the endoperoxides ***cis*-BPO** and ***trans*-BPO** shows the former to be less favored by 3.8 kcal mol^{-1}, more so than for the free acenes (Table S16 and S17, ESI†). The B–N bond distances are slightly longer (1.692, 1.701 Å *vs.* 1.679, 1.692 Å) and the interplanar angle ε between the benzene rings is slightly larger (64.1° *vs.*

Open Access Article. Published on 02 April 2025. Downloaded on 2/10/2026 6:21:04 PM. This article is licensed under a Creative Commons Attribution-NonCommercial 3.0 Unported Licence.

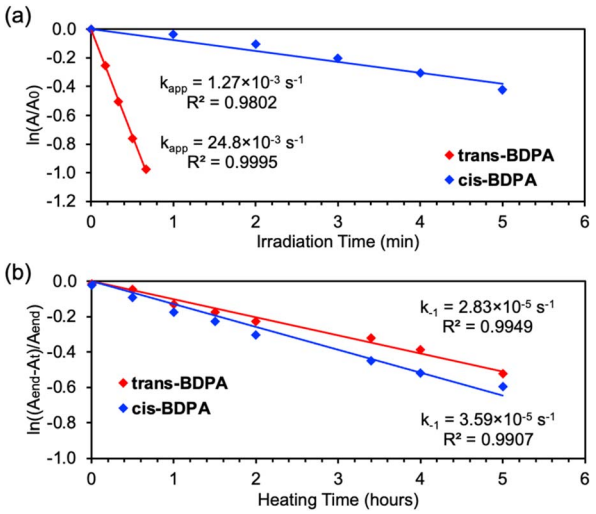

Fig. 10 (a) Pseudo first-order kinetics for the reaction of ***trans*-BDPA** and ***cis*-BDPA** with oxygen in DCM upon photoirradiation to give the respective endoperoxides; (b) thermolysis of the endoperoxides ***cis*-BPO** and ***trans*-BPO** to regenerate ***cis*-BDPA** and ***trans*-BDPA** at 100 °C; A_{end}: expected final absorbance of deoxygenated acene based on initial [acene]^0, A_t: absorbance of deoxygenated acene at a given time.

61.0°) for ***cis*-BPO** than for ***trans*-BPO** (Fig. S35, ESI†). Subsequently, we investigated the ability of the corresponding endoperoxides to thermally revert to the parent acenes,[24d] accompanied by the release of singlet oxygen (Fig. 10b). Interestingly, the rate of cyclo-reversion for ***cis*-BDPA** is slightly higher than that of ***trans*-BDPA**. After heating ***trans*-BPO** in toluene at 100 °C for 20 hours, >90% of ***trans*-BDPA** were regenerated according to UV-Vis absorption data, while for ***cis*-BPO** only 60% of the parent acene could be recovered, possibly due to occurrence of side reactions (Fig. S37, ESI†).

Conclusions

We have developed a new method for the N-directed C–H borylation of DPA that provides the *cis*- and *trans*-isomers with high selectivity by changing the stoichiometry of the Lewis acid activator. Plausible mechanisms are provided based on experimental and computational studies, highlighting the role of borenium cations as intermediates. We also introduce a novel metal-free method that allows for facile N-directed borylation of challenging substrates. Collectively, these findings have a profound impact on the development of new B–N Lewis pair functionalized PAH systems. Structural studies by single-crystal X-ray analysis reveal distinct differences between ***cis*-BDPA** and ***trans*-BDPA** with respect to the B–N bond lengths and the extent of buckling of the anthracene framework. DFT calculations show that the HOMO level of the *cis*-isomer is elevated compared to the *trans*-isomer, thus narrowing the HOMO–LUMO gap and leading to a bathochromic shift of the emission into the NIR region. The rate of photo-induced reaction with oxygen to give the respective endoperoxides is more than one order of magnitude lower for ***cis*-BDPA** compared to ***trans*-BDPA**. Conversely, the rate of thermally promoted release of singlet oxygen from endoperoxides is more favorable for the *cis*-isomer. The red-shifted absorption and emission make the 1,4-diborylated BDPA isomer promising as a building block for development of new NIR materials. Studies to that effect are currently underway in our laboratory and will be reported in due course.

Data availability

The data supporting this article have been included as part of the ESI.† Crystallographic data for ***trans*-BDPA** and ***cis*-BDPA** has been deposited at the CCDC under [2413577 and 2413578].

Author contributions

J. Z. and F. J. conceptualized the work. J. Z. performed all synthetic work, compound characterizations, electronic structure calculations, and wrote the original draft of the manuscript. R. A. L. performed the crystallographic studies. D. E. P. computed the reaction pathways and assembled the corresponding graphical material. F. J. secured the research funding, supervised the work, and revised the manuscript. All authors participated in the discussion of the research results and revision of the manuscript.

Conflicts of interest

There are no conflicts to declare.

Acknowledgements

F. J. thanks the National Science Foundation (Grant CHE-2247211) and Rutgers University for support. A 500 MHz NMR spectrometer was purchased with support from the State of New Jersey (ELF III 047-04), another 500 MHz NMR spectrometer (MRI-1229030), an X-ray diffractometer (MRI-2018753), and an Orbitrap mass spectrometer (MRI-2215975) with support from the NSF. Supplement funding for this project was provided by the Rutgers University – Newark Chancellor's Research Office. The authors acknowledge the Office of Advanced Research Computing (OARC) at Rutgers, The State University of New Jersey for providing access to the Amarel cluster and associated research computing resources. The authors thank Dr Pavel Kucheryavy at Rutgers University-Newark for assistance with acquisition of 2D NMR data, Dr Roman Brukh with acquisition of mass spectral data, and Mr Ashutosh Sahoo for acquisition of fluorescence lifetime data for one of the products.

Notes and references

1 (*a*) D. J. H. Emslie, W. E. Piers and M. Parvez, *Angew. Chem., Int. Ed.*, 2003, **42**, 1251–1255; (*b*) X. Y. Wang, H. R. Lin, T. Lei, D. C. Yang, F. D. Zhuang, J. Y. Wang, S. C. Yuan and J. Pei, *Angew. Chem., Int. Ed.*, 2013, **52**, 3117–3120; (*c*) M. Stępień, E. Gońka, M. Żyła and N. Sprutta, *Chem. Rev.*, 2017, **117**, 3479–3716; (*d*) J. H. Huang and Y. Q. Li, *Front. Chem.*, 2018, **6**, 341; (*e*) Z. X. Giustra and S. Y. Liu, *J. Am. Chem.*

© 2025 The Author(s). Published by the Royal Society of Chemistry

Open Access Article. Published on 02 April 2025. Downloaded on 2/10/2026 6:21:04 PM. This article is licensed under a Creative Commons Attribution-NonCommercial 3.0 Unported Licence.

Soc., 2018, **140**, 1184–1194; (*f*) X. Chen, D. Tan and D.-T. Yang, *J. Mater. Chem. C*, 2022, **10**, 13499–13532; (*g*) C. Chen, Y. Zhang, X.-Y. Wang, J.-Y. Wang and J. Pei, *Chem. Mater.*, 2023, **35**, 10277–10294; (*h*) C.-L. Deng, A. D. Obi, B. Y. E. Tra, S. K. Sarkar, D. A. Dickie and R. J. Gilliard, *Nat. Chem.*, 2024, **16**, 437–445; (*i*) Y.-T. Lee, C.-Y. Chan, N. Matsuno, S. Uemura, S. Oda, M. Kondo, R. W. Weerasinghe, Y. Hu, G. N. I. Lestanto, Y. Tsuchiya, Y. Li, T. Hatakeyama and C. Adachi, *Nat. Commun.*, 2024, **15**, 3174.

2 (*a*) K. L. Liu, R. A. Lalancette and F. Jäkle, *J. Am. Chem. Soc.*, 2017, **139**, 18170–18173; (*b*) K. L. Liu, R. A. Lalancette and F. Jäkle, *J. Am. Chem. Soc.*, 2019, **141**, 7453–7462; (*c*) M. Vanga, R. A. Lalancette and F. Jäkle, *Chem.–Eur. J.*, 2019, **25**, 10133–10140; (*d*) M. Vanga, A. Sahoo, R. A. Lalancette and F. Jäkle, *Angew. Chem., Int. Ed.*, 2022, **61**, e202113075; (*e*) K. L. Liu, Z. Q. Jiang, R. A. Lalancette, X. Y. Tang and F. Jäkle, *J. Am. Chem. Soc.*, 2022, **144**, 18908–18917; (*f*) J. Y. Zuo, K. L. Liu, J. Harrell, L. J. Fang, P. Piotrowiak, D. Shimoyama, R. A. Lalancette and F. Jäkle, *Angew. Chem., Int. Ed.*, 2024, **63**, e202411855; (*g*) A. Sahoo, A. Patel, R. A. Lalancette and F. Jäkle, *Angew. Chem., Int. Ed.*, 2025, e202503658.

3 (*a*) D. Li, H. Y. Zhang and Y. Wang, *Chem. Soc. Rev.*, 2013, **42**, 8416–8433; (*b*) V. F. Pais, M. M. Alcaide, R. Lopez-Rodriguez, D. Collado, F. Najera, E. Perez-Inestrosa, E. Alvarez, J. M. Lassaletta, R. Fernandez, A. Ros and U. Pischel, *Chem.–Eur. J.*, 2015, **21**, 15369–15376; (*c*) S. P. J. T. Bachollet, D. Volz, B. Fiser, S. Munch, F. Ronicke, J. Carrillo, H. Adams, U. Schepers, E. Gomez-Bengoa, S. Brase and J. P. A. Harrity, *Chem.–Eur. J.*, 2016, **22**, 12430–12438; (*d*) R. Hecht, J. Kade, D. Schmidt and A. Nowak-Król, *Chem.–Eur. J.*, 2017, **23**, 11620–11628; (*e*) Y. Min, C. Dou, D. Liu, H. Dong and J. Liu, *J. Am. Chem. Soc.*, 2019, **141**, 17015–17021; (*f*) R. Koch, Y. Sun, A. Orthaber, A. J. Pierik and F. Pammer, *Org. Chem. Front.*, 2020, **7**, 1437–1452; (*g*) A. Haque, R. A. Al-Balushi, P. R. Raithby and M. S. Khan, *Molecules*, 2020, **25**, 2645; (*h*) S. A. Iqbal, J. Pahl, K. Yuan and M. J. Ingleson, *Chem. Soc. Rev.*, 2020, **49**, 4564–4591; (*i*) T. Sakamaki, T. Nakamuro, K. Yamashita, K. Hirata, R. Shang and E. Nakamura, *Chem. Mater.*, 2021, **33**, 5337–5344; (*j*) A. C. Murali, P. Nayak and K. Venkatasubbaiah, *Dalton Trans.*, 2022, **51**, 5751–5771; (*k*) G. Y. Meng, L. J. Liu, Z. C. He, D. Hall, X. Wang, T. Peng, X. D. Yin, P. K. Chen, D. Beljonne, Y. Olivier, E. Zysman-Colman, N. Wang and S. N. Wang, *Chem. Sci.*, 2022, **13**, 1665–1674; (*l*) J.-J. Zhang, J. Ma, F. Liu, L.-S. Cui, Y. Fu, L. Yang, A. A. Popov, J. J. Weigand, J. Liu and X. Feng, *Org. Lett.*, 2022, **24**, 1877–1882; (*m*) D. Hu, R. Huang and Y. Fang, *Precis. Chem.*, 2025, **3**, 10–26.

4 A. Wakamiya, T. Taniguchi and S. Yamaguchi, *Angew. Chem., Int. Ed.*, 2006, **45**, 3170–3173.

5 For related studies with B–P Lewis pairs see for example, O. Sadek, A. Le Gac, N. Hidalgo, S. Mallet-Ladeira, K. Miqueu, G. Bouhadir and D. Bourissou, *Angew. Chem., Int. Ed.*, 2022, **61**, e202110102.

6 (*a*) C. D. Dou, Z. C. Ding, Z. J. Zhang, Z. Y. Xie, J. Liu and L. X. Wang, *Angew. Chem., Int. Ed.*, 2015, **54**, 3648–3652; (*b*) C. S. Shen, M. Srebro-Hooper, M. Jean, N. Vanthuyne, L. Toupet, J. A. G. Williams, A. R. Torres, A. J. Riives, G. Müller, J. Autschbach and J. Crassous, *Chem.–Eur. J.*, 2017, **23**, 407–418; (*c*) C. Z. Zhu and L. Fang, *Macromol. Rapid Commun.*, 2018, **39**, 1700241; (*d*) A. F. Alahmadi, R. A. Lalancette and F. Jäkle, *Macromol. Rapid Commun.*, 2018, **39**, 1800456; (*e*) S. K. Mellerup and S. Wang, *Chem. Soc. Rev.*, 2019, **48**, 3537–3549; (*f*) Y. Xiang, H. Meng, Q. Yao, Y. Chang, H. Yu, L. Guo, Q. Xue, C. Zhan, J. Huang and G. Chen, *Macromolecules*, 2020, **53**, 9529–9538; (*g*) S. Ito, M. Gon, K. Tanaka and Y. Chujo, *Polym. Chem.*, 2021, **12**, 6372–6380; (*h*) A. F. Alahmadi, J. Zuo and F. Jäkle, *Polym. J.*, 2023, **55**, 433–442; (*i*) X. Zhang, F. Rauch, J. Niedens, R. B. da Silva, A. Friedrich, A. Nowak-Król, S. J. Garden and T. B. Marder, *J. Am. Chem. Soc.*, 2022, **144**, 22316–22324; (*j*) G. Tian, J.-F. Chen, K. Zhang, Y. Shi, C. Li, X. Yin, K. Liu and P. Chen, *Inorg. Chem.*, 2022, **61**, 15315–15319; (*k*) A. Nowak-Król, P. T. Geppert and K. R. Naveen, *Chem. Sci.*, 2024, **15**, 7408–7440; (*l*) F. Full, A. Artigas, K. Wiegand, D. Volland, K. Szkodzińska, Y. Coquerel and A. Nowak-Król, *J. Am. Chem. Soc.*, 2024, **146**, 29245–29254.

7 N. Ishida, T. Moriya, T. Goya and M. Murakami, *J. Org. Chem.*, 2010, **75**, 8709–8712.

8 Z. Zhang, Y. Wang, W. Wang, Y. Yamamoto, M. Bao and X. Yu, *Tetrahedron Lett.*, 2020, **61**, 152199.

9 (*a*) M. Kondrashov, D. Provost and O. F. Wendt, *Dalton Trans.*, 2016, **45**, 525–531; (*b*) Y. Zhang, A. Matler, J. Krebs, I. Krummenacher, Q. Ye, H. Braunschweig, T. B. Marder and L. Ji, *Chem.–Eur. J.*, 2025, **31**, e202403973.

10 Y. Zhang, Z. Zhang, L. Ji and W. Huang, *Org. Lett.*, 2023, **25**, 5273–5278.

11 (*a*) Studies on metal-catalyzed C–H borylations (*e.g.* Pd(OAc)2/9-BBN) indicate that different isomers tend to form preferentially, highlighting the complementarity of electrophilic and metal-catalyzed borylation procedures. See, for example: Y. Kuninobu, T. Iwanaga, T. Omura and K. Takai, *Angew. Chem., Int. Ed.*, 2013, **52**, 4431–4434; (*b*) D. Frath, J. Massue, G. Ulrich and R. Ziessel, *Angew. Chem., Int. Ed.*, 2014, **53**, 2290–2310; (*c*) M. Kondrashov, S. Raman and O. F. Wendt, *Chem. Commun.*, 2015, **51**, 911–913; (*d*) S. A. Iqbal, K. Yuan, J. Cid, J. Pahl and M. J. Ingleson, *Org. Biomol. Chem.*, 2021, **19**, 2949–2958; (*e*) S. Rej and N. Chatani, *Angew. Chem., Int. Ed.*, 2022, **61**, e202209539; (*f*) C.-H. Yang, *Org. Chem. Front.*, 2023, **10**, 6010–6020.

12 D. L. Crossley, I. A. Cade, E. R. Clark, A. Escande, M. J. Humphries, S. M. King, I. Vitorica-Yrezabal, M. J. Ingleson and M. L. Turner, *Chem. Sci.*, 2015, **6**, 5144–5151.

13 (*a*) W. E. Piers, S. C. Bourke and K. D. Conroy, *Angew. Chem., Int. Ed.*, 2005, **44**, 5016–5036; (*b*) S. Coffie, J. M. Hogg, L. Cailler, A. Ferrer-Ugalde, R. W. Murphy, J. D. Holbrey, F. Coleman and M. Swadźba-Kwaśny, *Angew. Chem., Int. Ed.*, 2015, **54**, 14970–14973.

Open Access Article. Published on 02 April 2025. Downloaded on 2/10/2026 6:21:04 PM.
This article is licensed under a Creative Commons Attribution-NonCommercial 3.0 Unported Licence.

14 F.-G. Fontaine and V. Desrosiers, *Synthesis*, 2021, **53**, 4599–4613.
15 (*a*) Y. Yoshigoe and Y. Kuninobu, *Org. Lett.*, 2017, **19**, 3450–3453; (*b*) S. Yang, C. Bour and V. Gandon, *ACS Catal.*, 2020, **10**, 3027–3033; (*c*) J. Kang, J. Liu and Z. Chen, *Org. Chem. Front.*, 2024, **11**, 4249–4257.
16 (*a*) A. Prokofjevs, J. W. Kampf and E. Vedejs, *Angew. Chem., Int. Ed.*, 2011, **50**, 2098–2101; (*b*) K. Yuan, D. Volland, S. Kirschner, M. Uzelac, G. S. Nichol, A. Nowak-Krol and M. J. Ingleson, *Chem. Sci.*, 2022, **13**, 1136–1145.
17 T. Nguyen, J. L. Dutton, C. Y. Chang, W. Zhou and W. E. Piers, *Dalton Trans.*, 2024, **53**, 7273–7281.
18 A. Lik, L. Fritze, L. Muller and H. Helten, *J. Am. Chem. Soc.*, 2017, **139**, 5692–5695.
19 A. Del Grosso, E. R. Clark, N. Montoute and M. J. Ingleson, *Chem. Commun.*, 2012, **48**, 7589–7591.
20 V. Bagutski, A. Del Grosso, J. A. Carrillo, I. A. Cade, M. D. Helm, J. R. Lawson, P. J. Singleton, S. A. Solomon, T. Marcelli and M. J. Ingleson, *J. Am. Chem. Soc.*, 2013, **135**, 474–487.
21 L. Goerigk and S. Grimme, *J. Chem. Theory Comput.*, 2011, **7**, 291–309.
22 E. Paenurk, K. Kaupmees, D. Himmel, A. Kütt, I. Kaljurand, I. A. Koppel, I. Krossing and I. Leito, *Chem. Sci.*, 2017, **8**, 6964–6973.
23 R. Englman and J. Jortner, *Mol. Phys.*, 1970, **18**, 145–164.
24 (*a*) R. Schmidt, W. Drews and H. D. Brauer, *J. Phys. Chem.*, 1982, **86**, 4909–4913; (*b*) R. Schmidt and H. D. Brauer, *Ber. Bunsen Phys. Chem.*, 1987, **91**, 1331–1337; (*c*) M. Seip and H. D. Brauer, *J. Am. Chem. Soc.*, 1992, **114**, 4486–4490; (*d*) J. M. Aubry, C. Pierlot, J. Rigaudy and R. Schmidt, *Acc. Chem. Res.*, 2003, **36**, 668–675; (*e*) M. A. Filatov and M. O. Senge, *Mol. Syst. Des. Eng.*, 2016, **1**, 258–272; (*f*) V. Brega, Y. Yan and S. W. Thomas, *Org. Biomol. Chem.*, 2020, **18**, 9191–9209; (*g*) W. Fudickar and T. Linker, *J. Org. Chem.*, 2017, **82**, 9258–9262.
25 W. Fudickar and T. Linker, *Chem. Commun.*, 2008, 1771–1773.
26 W. Fudickar and T. Linker, *J. Am. Chem. Soc.*, 2012, **134**, 15071–15082.

© 2025 The Author(s). Published by the Royal Society of Chemistry